Journal of Materials Chemistry B

PAPER

View Article Online
View Journal

Cite this: DOI: 10.1039/c6tb03101c

Crystal structure dependent *in vitro* antioxidant activity of biocompatible calcium gallate MOFs†

Tania Hidalgo,‡[a] Lucy Cooper,‡[a] Martin Gorman,[a] Tamara Lozano-Fernández,[b] Rosana Simón-Vázquez,[b] Georges Mouchaham,[a] Jérome Marrot,[a] Nathalie Guillou,[a] Christian Serre,§[a] Pierre Fertey,[c] África González-Fernández,[b] Thomas Devic¶*[a] and Patricia Horcajada ‖*[a]

Received 29th November 2016,
Accepted 14th March 2017

DOI: 10.1039/c6tb03101c

rsc.li/materials-b

Two novel 3-D coordination polymers, denoted MIL-155 and MIL-156 (MIL stands for Materials Institute Lavoisier), built up from calcium and the naturally occurring gallic acid (H_4gal), have been hydrothermally synthesized and their crystal structures were determined by single-crystal X-ray diffraction. These solids are based on different inorganic subunits: infinite chains of edge-sharing dimers of CaO_7 polyhedra linked through partially deprotonated gallate ligands (H_2gal^{2-}) for MIL-155 or $[Ca_2(H_2O)(H_2gal)_2]\cdot 2H_2O$, and ribbon-like inorganic subunits containing both eight-fold or six-fold coordinated Ca^{II} ions linked through fully deprotonated gallate ligands (gal^{4-}) for MIL-156 or $[Ca_3K_2(H_2O)_2(gal)_2]\cdot nH_2O$ ($n \sim 5$). Both solids contain small channels filled with water molecules, with, however no accessible porosity towards N_2 at 77 K. MIL-155 and MIL-156 were proven to be biocompatible, as evidenced by *in vitro* assays (viability and cell proliferation/death balance). While the high chemical stability of MIL-156 makes it almost bioinert, the progressive degradation of MIL-155 leads to an important protective antioxidant effect, associated with the release of the bioactive gallate ligand.

Introduction

Over the past twenty years, porous coordination polymers (PCPs) or metal organic frameworks (MOFs) have been widely studied with regard to various potential applications, mostly associated with the sorption properties of these materials.[1–3] Besides conventional applications in the fields of fluid storage/separation or catalysis, bio-related properties have recently attracted much attention.[4–6] While MOFs were initially considered as carriers for the delivery of diverse active ingredients (AIs),[7] other areas of application have also emerged, such as bio-imaging,[8] sensing[9,10] or enzyme immobilization.[11] Although the traditional use of MOFs as drug carriers is based on the adsorption/desorption of the AIs within the MOF porosity, the incorporation of the AIs as a constitutive part of the hybrid framework has recently attracted great attention.[12–16] This latest strategy allows not only to tune the release of the AI through the degradation of the network, which strongly depends on the metal/ligand pair and the structure, but also avoids the possible toxicity inherent to the exogenous compounds (*i.e.* cations or ligands), typically used for the MOF synthesis. Therefore, it is generally accepted that the combination of abundant endogenous cations (M = Zn, Fe, Mg, Ca,...) and naturally occurring ligands,[17] using non-toxic solvents, is an appealing strategy to achieve more sustainable biofriendly materials.

Calcium is a particularly advantageous candidate for biomedical applications due to its low cost and abundant presence in the body ($\sim$1 kg in the average human body) together with its high recommended intake ($\sim$1 g per day).[18,19] In particular, calcium is involved in bone health and other important physiological processes such as enzyme activation, nerve impulse transmission, hypertension, obesity modulation and muscle contraction, among others.[20–22]

[a] *Institut Lavoisier, UMR 8180 CNRS Université de Versailles Saint-Quentin-en-Yvelines, 45 avenue des Etats-Unis, 78035 Versailles cedex, France. E-mail: thomas.devic@cnrs-imn.fr*

[b] *Immunology, Biomedical Research Center (CINBIO) and Institute of Biomedical Research of Vigo (IBIV), Universidad de Vigo, Campus Lagoas Marcosende, 36310 Vigo, Pontevedra, Spain*

[c] *Synchrotron Soleil, beamline Cristal, L'Orme des Merisiers, Saint-Aubin, 91192 Gif-sur-Yvette cedex, France*

† Electronic supplementary information (ESI) available: Experimental data including detailed synthetic procedures, characterization (XRD, IR spectra, crystallography data, bond valence calculations) for both MOFs as well as the ROS production, annexin and cytotoxicity assays of each one and their precursor. CCDC 1519913 and 1519914. For ESI and crystallographic data in CIF or other electronic format see DOI: 10.1039/c6tb03101c

‡ These authors contributed equally to this work.

§ Current address: Institut des Matériaux Poreux de Paris, FRE 2000 CNRS Ecole Normale Supérieure – Ecole Supérieure de Physique et de Chimie Industrielles de Paris, Paris Research University, Paris, France.

¶ Current address: Institut des Matériaux Jean Rouxel, UMR 6502 CNRS Université de Nantes, 2 rue de la Houssinière, 44322 Nantes cedex 3, France.

‖ Current address: IMDEA Energy. Av. Ramón de la Sagra 3, 28935 Móstoles, Madrid, Spain. E-mail: patricia.horcajada@imdea.org

Amongst the large panel of biologically occurring or bioactive molecules potentially used as ligands (nucleobases,[23] carboxylates,[24–26] carbohydrates,[27] amino acids, small peptides[28]), phenolic derivatives[29,30] also appear to be suitable spacers due to their natural abundance and their known antioxidant activity.[31,32] In particular, gallic acid (H_4gal) is an abundant naturally occurring hydroxycarboxylic acid with interesting antioxidant properties, associated with various beneficial therapeutic effects, including anti-allergic, -inflammatory, -viral,[33] -fungal, -microbial[34] and even -carcinogenic,[35,36] as well as cardio[37] and neuro-protective[38] activities.

However, to the best of our knowledge, while several 1-D coordination polymers built up from this ligand and Zr^{IV} have been structurally characterized,[39,40] only one structure type of 3-D metal (M) gallate has been reported so far. It consists of infinite chains of corner-sharing MO_6 octahedra connected through gallate ligands to define triangular shaped channels. This solid can be prepared from various cations (Fe^{III}, Co^{II}, Ni^{II}, Mn^{II} or Mg^{II}) and is formulated as Fe(galH)·$2H_2O$ or M^{II}(galH_2)·$2H_2O$.[41–43] We recently showed that the Mg^{II} analogue combines an accessible microporosity together with a high biocompatible character and a strong antioxidant activity for promyelocytic leukemic cells HL-60.[43] With this in mind, we extended our study by exploring the reactivity of gallic acid with another non-toxic cation (here calcium), in order to assess the impact of the composition and structure on the bioactivity of such materials.

Herein, we report the synthesis under hydrothermal conditions of two novel 3-D calcium gallate coordination polymers. Both crystal structures were solved by single-crystal X-ray diffraction (XRD) and the solids were further characterized by infrared (IR) spectroscopy, thermogravimetric analysis (TGA), N_2 porosimetry and temperature dependent powder XRD. In addition, their chemical stability was evaluated, both in water and in a more complex simulated physiological medium. Finally, the potential protective antioxidant bioactivity of these solids was assessed by means of the reactive oxygen species (ROS) production, investigating their *in vitro* biocompatibility by different cellular viability and cell proliferation/death balance assays.

Experimental section

Materials

Gallic acid monohydrate ($C_7H_6O_5$·H_2O) (Sigma Aldrich, ≥98.0%), calcium nitrate tetrahydrate [$Ca(NO_3)_2$]·$4H_2O$ (Carlo Erba Reagents, 99.0–103.0%), calcium hydroxide $Ca(OH)_2$ (Aldrich 95%) and KOH pellets (Alfa Aesar, 85%) were obtained commercially and used without any further purification. Phosphate buffered saline (PBS) solution (0.01 M, pH = 7.4), RPMI 1640 medium supplemented with GlutaMAX™, penicillin–streptomycin (5000 U mL^{-1}) and heat-inactivated fetal bovine serum (FBS) were provided by Gibco®-Life Technologies (see ref. 44 for composition). Similarly, dimethylsulfoxide (DMSO; ≥99.7%) and thiazolyl blue tetrazolium bromide (MTT) were purchased from Sigma Aldrich (St Louis, MO), whereas the phorbol 12-myristate-13-acetate (PMA) was provided by Abcam Biochemicals, H_2O_2 (30% w/v) by Panreac (Barcelona, Spain), 2′,7′-dichlorofluorescein diacetate (2.5 μM; DCFH-DA) by Invitrogen™ and the Annexin V-FITC Apoptosis Detection Kit was supplied by Immunostep (Salamanca, Spain). All materials were used as received without further purification.

Synthesis

Crystals suitable for single crystal X-ray diffraction analysis were synthesised hydrothermally at 120 °C, although MIL-155 could also be synthesised under reflux as a microcrystalline powder.

MIL-155: [$Ca_2(H_2O)(H_2gal)_2$]·$2H_2O$. Gallic acid monohydrate (0.376 g, 2 mmol) was dissolved in distilled water (10 mL) at room temperature. Calcium nitrate (0.236 g, 1 mmol) was then added to the solution followed by a KOH 5 M aqueous solution which was added dropwise until the solution reached pH ∼ 8/9 (∼800 μL = ∼4 mmol).

The reaction mixture was then sealed in a Teflon lined autoclave reactor, placed in an oven, heated up to 120 °C in 1 h, and then kept at this temperature for 12 h; the final pH value was 8. Once cooled to room temperature the resulting crystalline powder was filtered, repeatedly washed with distilled water and dried at room temperature. This solid could also be synthesised under reflux on a larger scale: Gallic acid monohydrate (1.881 g, 10 mmol) was dissolved in distilled water (100 mL) at room temperature. Calcium nitrate (1.181 g, 5 mmol) was then added to the solution followed by a KOH 5 M solution which was added dropwise until the solution reached pH 9. The reaction solution was heated under reflux for 24 h.

MIL-156: [$Ca_3K_2(H_2O)_2(gal)_2$]·$n H_2O$ (n = 4–6). Gallic acid monohydrate (0.188 g, 1 mmol) was dissolved in distilled water (10 mL) at room temperature. Calcium hydroxide (0.074 g, 1 mmol) was then added to the solution followed by a KOH 5 M solution which was added dropwise until the solution reached pH 14 (∼800 μL = ∼4 mmol). The reaction mixture was then sealed in a Teflon lined autoclave reactor, placed in an oven, heated up to 120 °C in 1 h, and then kept at this temperature for 24 h; the final pH was ∼14. Once cooled to room temperature the resulting solid was filtered, repeatedly washed with distilled water and dried at room temperature to reveal needle like crystals.

Single crystal X-ray diffraction

MIL-155: [$Ca_2(H_2O)(H_2gal)_2$]·$2H_2O$. The crystals were too small to be studied using a conventional laboratory diffractometer. The structure was then determined for a microcrystal (dimensions: 0.02 × 0.02 × 0.004 mm; Table S1, ESI†) from the data collected on the CRISTAL beamline at Synchrotron Soleil, using a set up adapted for small crystals at 100(2) K on an Xcalibur Atlas four-circle diffractometer and equipped with a CCD plate detector. Data reduction was performed using CrysAlis. An empirical absorption correction was applied using spherical harmonics on the basis of multiple scans of equivalent reflections, implemented in the SCALE3 ABSPACK scaling algorithm.

MIL-156: $[Ca_3K_2(H_2O)_2(gal)_2]\cdot nH_2O$ (n = 4–6). For MIL-156, the crystals were of sufficient size to be measured using a laboratory diffractometer. The chosen crystal (dimensions: 0.2 × 0.04 × 0.03 mm; Table S1, ESI†) was analysed at room temperature 293(2) K using a Bruker Nonius X8 APEX diffractometer equipped with a CCD area detector. SAINT software was used to integrate and scale intensities and a semi-empirical absorption correction (SADABS) was applied on the basis of multiple scans of equivalent reflections.

The structures of both MIL-155 and MIL-156 were solved by direct methods using SHELXS-97 and refined with the full matrix least squares routine SHELXL-97. Non H-atoms were refined anisotropically. The aromatic protons attached to gallate ligands were added as rigid bodies whilst acidic hydrogen atoms and the ones bound to the water molecules in MIL-155 were located using difference Fourier maps, taking into account the results of the bond valence calculation (see the discussion below). The exact positions of the protons in the water molecules in MIL-156 have not been determined.

Crystallographic and refinement parameters are summarised in Table S1 (ESI†).

Physicochemical characterisation

TGA analysis was carried out using Mettler Toledo TGA/DSC 1, STAR®System apparatus under O_2, at a heating rate of 3 °C min^{-1} up to 800 °C. X ray powder diffraction (XRPD) patterns were collected at 293 K on a Siemens D5000 Diffractometer working in the (θ–2θ) mode by using CuKα radiation. X-ray thermodiffraction was performed using a θ–θ Bruker D8 Advance diffractometer equipped with a HTK-1200N (Anton Parr) high temperature chamber and a LYNXEYE XE detector (Cu radiation). Diagrams were collected every 10 °C between 20 and 300 °C. IR spectra were recorded using a Nicolet 6700 FT-IR Thermo Scientific spectrometer between 500 and 4000 cm^{-1} (Fig. S2, ESI†).

Prior to the N_2 sorption measurements, samples were heated overnight at 100 °C under primary vacuum (BEL Japan, BELSORP Prep). Then, N_2 sorption isotherms were collected at 77 K on a BEL Japan Belsorp Mini apparatus.

Degradation tests

The release of gallic acid from $Mg(H_2gal)$, MIL-155 and MIL-156 was performed in triplicate (corresponding to the average obtained in two independent experiments [n = 6] and the error bars corresponding to the standard deviation) by soaking 12 mg of each solid in 12 mL of aqueous solution (Milli-Q water) and in a cell culture medium (RPMI) at 37 °C under continuous stirring. After different incubation times (1, 4, 8 and 24 h), an aliquot of the supernatant was recovered by centrifugation (14 500 rpm, 15 min). The monitoring of the gallic acid release was carried out through a reversed phase high performance liquid chromatography (HPLC) system from Waters (Waters Alliance E2695 separations module) with a Sunfire-C18 reverse-phase column (5 μm, 4.6 × 150 mm from Waters) and equipped with a Waters 2998 variable-wavelength photodiode array detector, controlled using Empower software. The mobile phase used for the measurements consisted of a mixture of 45% v/v methanol in PBS solution (0.04 M, pH 2.5), injecting 10 μL as the sample volume under a flow rate of 1 mL min^{-1} and with 25 °C as the column temperature. Different solutions of free gallic acid were analysed as standards for the calibration curve in the range of 1.00–0.01 mg mL^{-1} (correlation coefficient > 0.99). Note that the limit of quantification of gallic acid was estimated to be 3.7 mg mL^{-1}. A chromatogram of the standards showed a retention time for gallic acid at 2.7 min with an absorption maximum at 210 nm.[45,46] Finally, the degradation kinetics of $Mg(H_2gal)$, MIL-155 and MIL-156 were represented as the wt% of the linker released.

In vitro studies

Cells and culture. NCI-H460, RAW-264.7 and HL-60 cell lines (ATCC®HTB-177TM, ATCC®TIB-71TM and ATCC®CCL-240TM, respectively) were cultured in RPMI 1640 GlutaMAX™, supplemented with 10% FBS, and 100 units mL^{-1} of penicillin/streptomycin. Cell lines were grown at 37 °C in a humidified 5% CO_2 atmosphere.

Cytotoxicity assays. The cytotoxic activity of $Mg(H_2gal)$, MIL-155 and MIL-156 as well as their precursors ($Mg(OH)_2$, $Ca(NO_3)_2$, $Ca(OH)_2$ and H_4gal) was analysed by the MTT and Annexin assays.[47,48] Adherent NCI-H460 and RAW-264.7 cells were seeded 24 h prior to the assay in 96-well plates at a density of 1 × 10^4 cells per well in RPMI supplemented with 10% FBS. The HL-60 cell line, with cells in the suspension, was used directly at a density of 1 × 10^5 cells per well in RPMI supplemented with 10% FBS. The treatments were prepared at a 10-fold higher concentration (due to a direct 1/10 direct dilution in the well, as 30 μL of the sample in PBS were added to a final volume of 300 μL per well). Based on this first concentration, a dilution series of $Mg(H_2gal)$, MIL-155 and MIL-156 were performed with cell culture media, yielding different concentrations (from 250 to 1 μg mL^{-1}). Subsequently, all these stimuli were added to the cells for 24 h, keeping them at 37 °C under a 5% CO_2 atmosphere in both experiments. From one site, the cytotoxicity was determined by adding the MTT reactant (0.5 mg mL^{-1} in PBS, incubation at 37 °C for 2 h) after the contact time, followed by a PBS washing with 200 μL, ending with 100 μL of DMSO added to each well, together with their measurement of the absorbance (at λ = 539 nm) after stirring.[49] The results are summarised in Fig. S4 (ESI†). In addition, the cytotoxicity was measured by determination of the apoptotic and necrotic index after 24 h in contact with the treatment. The cells were analysed using an Annexin-V FITC kit (Immunostep, Salamanca, Spain), following manufacturer's instructions.[50,51] Briefly, after the contact of the cells with the material, they were stained with an Annexin probe, which binds to phosphatidylserine at the outer cell membrane, detecting cell apoptosis. Propidium iodide (PI) was used to quantify necrotic cells, since this dye stains DNA after the membrane becomes permeable to PI. Data acquisition and analysis were done by flow cytometry (BD Accuri™ C6, Biosciences) using Accuri software. For each analysis, 10000 events were acquired, detecting FITC and PI fluorescence in the green and red fluorescence channels, respectively. The results are summarised in Fig. S5 and S6 (ESI†).

ROS production. The cells were seeded in 96-well plates (U bottom) at a density of 1×10^5 cells per well in 100 μL of cell culture medium (RPMI supplemented with 10% FBS). The stimulus-containing solutions of 100 μL were added to the cells at final concentrations of 5, 15, 30 and 60 μg mL^{-1} of either MOFs such as $Mg(H_2gal)$, MIL-155 and MIL-156 or their precursors ($Mg(OH)_2$, $Ca(NO_3)_2$, $Ca(OH)_2$ and H_4gal). Basal and negative controls were considered as the cells in the absence of stimulus and the cells in the presence of a ROS reactant (2′,7′-dichlorofluorescein diacetate, DCFH-DA, Invitrogen™), respectively. As the positive control, the cells were incubated with an oxidant component, phorbol 12-myristate-13-acetate PMA (10 μM) at 37 °C. After 8 h of incubation, cells were centrifuged (900 rpm, 5 min) and kept in contact with the ROS reactant, (1 μL per 200 μL of cells) for 30 min at 37 °C under dark conditions. Two PBS-washes were performed after the incubation and, finally, the 2′,7′-dichlorofluorescein (DCF) fluorescence in cells was measured using flow cytometry (BD Accuri™ C6 Flow Cytometer) on the total living population region.[52,53] All data are presented in Fig. 5 and Fig. S3 (ESI†).

Results and discussion

Synthesis and crystal structures

The reactivity of H_4gal with calcium salts in water under hydrothermal conditions was thoroughly investigated. By systematically varying the pH of the reaction mixture (upon addition of a KOH solution), it was possible to isolate two crystalline phases, both in a pure form (see Fig. S1 (ESI†) for XRD powder patterns). The first compound, denoted as MIL-155 (MIL stands for Materials Institute Lavoisier), was isolated under slightly basic conditions with pH ranging from 7–8 to 10 (the best crystallinity at pH = 8–9), whereas pH ranging from 11 to 13 leads to an amorphous product and/or $CaCO_3$; a second hybrid solid, namely MIL-156, could be isolated under very basic conditions (pH = 14).

MIL-155: $[Ca_2(H_2O)(H_2gal)_2]\cdot 2H_2O$. As detailed below, single crystal X-ray diffraction analysis (see Table S1, ESI† for refinement details) revealed that both solids are 3-D coordination polymers. Nevertheless, both the nature of the inorganic subunits and the protonation state of the ligands differ. Furthermore, potassium ions are present in the structure of MIL-156 and absent from MIL-155.

MIL-155 crystallises in a triclinic setting, space group $P\bar{1}$, with two Ca (Ca1 and Ca2), two gallate (galA and galB) and three water molecules (Ow1, Ow2, Ow3) in a general position, leading to the formula $[Ca_2(H_2O)(H_2gal)_2]\cdot 2H_2O$. Both calcium cations are surrounded by 6 oxygen atoms from the ligands (both carboxylate and phenolate) and one water molecule (Ow1). The CaO_7 polyhedra connect to each other through both corners and edges to define double chains running parallel to the *a* axis (Fig. 1b). These inorganic chains are further interconnected through both galA and galB ligands, both parallel to the *b*, *c* plane to define small rectangular channels running along the *a* axis and containing free water molecules, namely

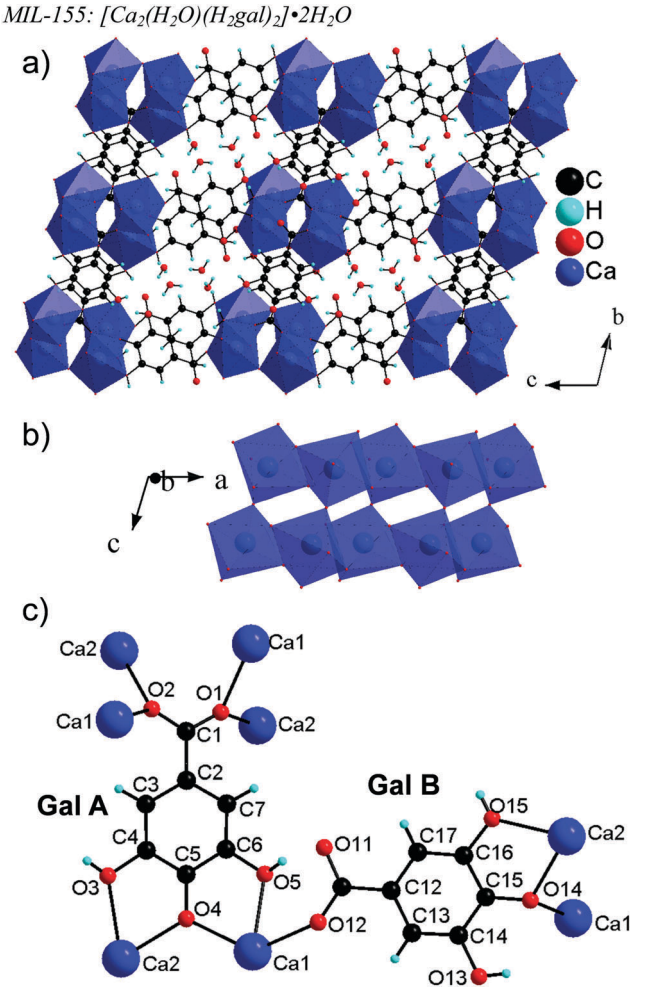

Fig. 1 Structure of MIL-155: (a) general view along the *a* axis; (b) double chain of corner and edge sharing CaO_7 polyhedra; (c) coordination feature of both independent gallate ligands.

Ow2 and Ow3 (Fig. 1a). As shown in Fig. 1c, both ligands adopt different coordination environments: galA is connected to six Ca cations (3 × Ca1, 3 × Ca2), two being chelated by the phenolic oxygen and four being connected through the carboxylate ones, whereas galB is coordinated to only three Ca ions (2 × Ca1, 1 × Ca2), two being connected through phenolic oxygens (one chelated, one singly bound), one through the carboxylate one. Structural analysis, in combination with IR spectroscopy, was further used to determine a plausible protonation state of the constituents. Bond valence calculation (see Table S2, ESI†) indicates that Ow1 is indeed a bridging water molecule rather than an anionic (OH^-, O^{2-}) ligand. Considering the Ca to ligand ratio (1 : 1), it is thus expected that the ligands are only partially deprotonated, with two acidic protons remaining (H_2gal^{2-}). Indeed, an adsorption band in the infrared spectrum at 3400 cm^{-1}, attributed to acidic O–H groups, confirms this hypothesis (Fig. S2, ESI†). For ligand H_2galA, bond valence calculations (Table S2, ESI†) suggest that both *meta*-phenoxy oxygen atoms (O3 and O5) are protonated, while other oxygen atoms (O1, O2, O4) are deprotonated, similar to what was found in the already reported solids $M^{II}(H_2gal)\cdot 2H_2O$.[41–43] The comparison of

the C–O bond lengths in both solids (Table S3, ESI†) also seems to support this finding. For ligand H_2galB, bond valence calculations only allowed us to establish the protonation state for the coordinated phenolic oxygen (O14 and O15): the *meta*-oxygen (O15) appears protonated, while the *para* one (O14) is deprotonated (Table S2, ESI†). For the uncoordinated *meta*-oxygen (O13), the examination of the C–O bond length (Table S3, ESI†) also suggests that it is protonated. Taking this assumption into account, the uncoordinated carboxylate oxygen must be deprotonated in order to reach an overall charge of −2. Partial disorder of the acidic proton cannot of course be ruled out. However, the examination of the IR spectrum, for which no band characteristic of the C=O vibration of a carboxylic acid group was detected (region 1700–1660 cm^{-1}, see Fig. S2, ESI†), further validates this model. Plausible positions of the hydrogen atoms bonded to *meta*-phenolic oxygens and of the water molecules were thus finally deduced from the Fourier map. The presence of both acidic protons of the ligand and bound and free water molecules leads to a complex hydrogen bond network involving all these constituents (see Table S4, ESI† for related distances and angles).

Although the protonation state of the gallate ligands and the formula of MIL-155 are similar to the known M(II) gallate solids,[41–43] both compounds are not isostructural. The difference mainly relies on the coordination state of the Ca ions: its larger ionic radius allowed a coordination number higher than six (here seven), hence leading to a completely different structure.

MIL-156: $[Ca_3K_2(H_2O)_2(gal)_2]\cdot nH_2O$ ($n \sim 4$–6). MIL-156 crystallises in an orthorhombic setting, space group *Pccn*, with one Ca ion lying on a two-fold axis, and one Ca cation, one K cation, one gallate ligand and four water molecules, among which one presents a 0.5 occupancy, in the general position, giving rise to the formula $[Ca_3K_2(H_2O)_2(gal)_2]\cdot nH_2O$, $n \sim 5$. One of the Ca ions (Ca1) is octahedrally coordinated by four ligand-related oxygen atoms and two water molecules (Ow1), whereas the second one (Ca2) is 8-fold coordinated solely by phenolic oxygens. Both polyhedra share edges to define inorganic ribbons running along the *c* axis (Fig. 2b). The gallate moieties connect these ribbons along the $a + b$ and $a - b$ directions to define a 3-D framework with channels running parallel to the ribbons and filled with both potassium ions and free water molecules (Fig. 2a). Each ligand interacts with six Ca ions (see Fig. 2c), with only one singlet oxygen (from the carboxylate group) not involved in the coordination bond. Again, bond valence calculation confirmed that Ow1 is a bridging water molecule and not an anionic ligand (Table S5, ESI†). Taking into account the formula, the gallate ligand must be totally deprotonated. This is again in reasonable agreement with bond valence calculation (Table S5, ESI†) and with the IR analysis, for which, in contrast to MIL-155, no acidic proton is detected in the 3400–3500 cm^{-1} region (Fig. S2, ESI†). This can, of course, be explained by the more basic synthetic conditions, implying a more negatively charged ligand, resulting in a higher M/L ratio, and hence a higher degree of inorganic condensation.[54]

Potassium ions are lying in the channels to balance the charge, interacting weakly with *meta*-phenolic oxygen atoms

MIL-156: $[Ca_3K_2(H_2O)_2(gal)_2]\cdot nH_2O$ ($n \sim 4$-6)

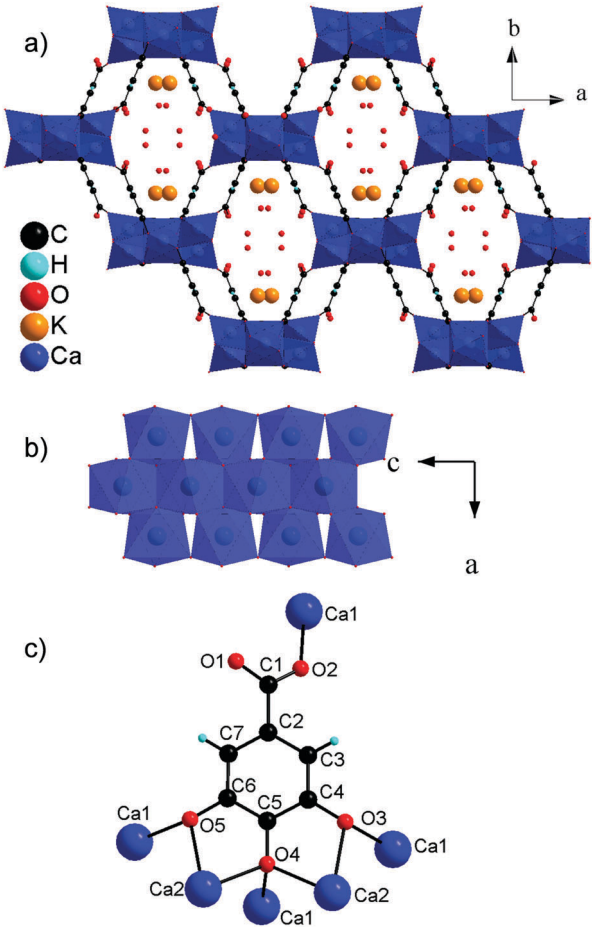

Fig. 2 Structure of MIL-156: (a) general view along the *c* axis; (b) ribbon of edge sharing CaO_6 and CaO_8 polyhedra; (c) coordination feature of the gallate ligand.

(see Table S5, ESI† for distances) and free water molecules. If one considers the structure along the *c* axis, one can point out that the potassium cation sits very close to the centre of the aromatic ring of the gallate ligand ($3.15 < d_{C\cdots K} < 3.41$ Å), hence suggesting the occurrence of an electrostatic supramolecular K^+–π interaction (Fig. S3, ESI†).[55] Finally, free and bound water molecules together with the pendant oxygen atom from the carboxylate group are involved in a 1-D hydrogen bond network deploying along the channel axis (see Table S6, ESI† for characteristic distances).

Physicochemical characterisation

In order to investigate the thermal behaviour of MIL-155 and MIL-156, both TGA and temperature dependent powder XRD experiments were carried out under oxygen and air atmospheres, respectively (see Fig. 3).

The TGA curve of MIL-155 (Fig. 3a) shows two weight losses below 200 °C (in the 60–100 and 140–190 °C ranges), associated with the departure of both free and bound water molecules (weight losses: obs. 10.5%, cal. 11.5%). Such departure leads to slight structural changes, as detected on the thermodiffractogram (Fig. 3b).

Above 230–250 °C, the combustion of the ligand gives rise to the collapse of the framework and the successive formation of $CaCO_3$ ($470 < T < 560$ °C, weight losses: obs. 53%, cal. 57%) and CaO ($T > 670$ °C, weight losses: obs. 74%, theo. 76%) is likely. For MIL-156, two weight losses, likely associated with the departure of most of the water molecules (weight losses: obs. 16%, cal. 14 and 19% for the departure of only free and both bound and free water molecules respectively) are also found below 150 °C (Fig. 3a). The second one is associated with a major structural modification (see Fig. 3c); the resulting compound, although less crystalline than the pristine one, remains ordered up to 300 °C. Above 150 °C, the TG curve (Fig. 3a) presents a slightly decreasing plateau up to 530 °C, followed by two major losses, likely leading to CaO and K_2CO_3 (weight losses: obs. 51%, cal. 53%).

As both MIL-155 and MIL-156 were found to present channels filled with water molecules, their porosity was evaluated by means of nitrogen adsorption measurements at 77 K. After activation under primary vacuum overnight at 100 °C, neither of them was found to adsorb a significant amount of nitrogen.

Bioactivity

Biocompatibility evaluation. The *in vitro* toxicity of different concentrations of MIL-155 and MIL-156 was firstly evaluated in three different cell lines (human promyelocytic leukaemia (HL-60), human non-small lung cancer (NCI-H460) and murine leukemic monocyte (RAW-264.7)) by means of the cell viability MTT assay (see the Experimental section). Remarkably, very low cytotoxicity profiles were observed after 24 h of cell contact time (Fig. S4, ESI†), associated with important values of the half maximal inhibitory concentration (IC_{50} = 125 and 250 μg mL^{-1} for MIL-155 and MIL-156, respectively, regardless of the cell line). The lower toxicity of MIL-156 could be related to its higher chemical stability (see below). Note here that totally comparable IC_{50} values were also obtained for the already reported $Mg(H_2gal)$.[43]

Then, in order to provide some information about the cell proliferation/cell death balance as well as the potential activation of a specific death pathway, Annexin-V-FITC assays[50,51] were carried out using the HL-60 cell line (see the Experimental section). In these studies, the living cells, early and late apoptosis cells (programmed cell death by normal and healthy process) together with necrotic cells (cell death that is triggered by external factors, such as trauma or infection) can be distinguished. At low concentrations ($\leq$30 μg mL^{-1}), both Ca gallates showed the high presence of living cells ($\geq$75% after 24 h, Fig. S5, ESI†). One can nevertheless point out a slight increase of the early apoptotic cells percentage in contact with intermediate concentrations (30–60 μg mL^{-1}), reaching a substantial late apoptotic state ($\sim$88%) for MIL-155 at higher concentrations ($\geq$60 μg mL^{-1}). On the other hand, MIL-156 exhibited similar patterns to $Mg(H_2gal)$,[43] with $\sim$50% of late apoptotic cells, observed at higher concentrations (125 μg mL^{-1}). These results are in accordance with the higher cell viability of MIL-156 when compared with MIL-155 (see above). Additional experiments, performed on the isolated constituents ($Ca(NO_3)_2$, $Ca(OH)_2$ and H_4gal; Fig. S6, ESI†), indicate that the cell toxicity observed at high concentrations arises from the ligand (20 *vs.* < 2% of apoptotic cells in H_4gal *vs.* the cation precursors, respectively). This is in agreement with previous data reported for the $Mg(H_2gal)$,[43] in which the high concentration of phenolic components was associated with a pro-oxidant behaviour, inducing the apoptotic cell death by oxidative degradation.[56]

On the whole, these solids seem to exhibit good *in vitro* biocompatibility.

Antioxidant activity and stability studies. Considering the probed antioxidant effect of the constitutive gallate ligand and our first results on the $Mg(H_2gal)$ solid,[43] the potential antioxidant activity of MIL-155 and MIL-156 was assessed by evaluating the production of Reactive Oxygen Species (ROS) from cells in contact with an increasing amount of MOF (from 5 to 60 μg mL^{-1}). The macrophage lineage HL-60 was selected here since it has been widely recommended as a model for the study of the cellular oxidation state.[53] Two controls were first considered: a positive control C+, incubating the cells with an oxidant molecule (ROS inducer), namely phorbol 12-myristate-13-acetate (PMA), and a negative control C−, incubating the cells without treatment. After 8 h contact time, the incubation with dichlorofluorescein diacetate (DCFH-DA, ROS reactant) allowed the revealing of the diverse oxidation states of the cells

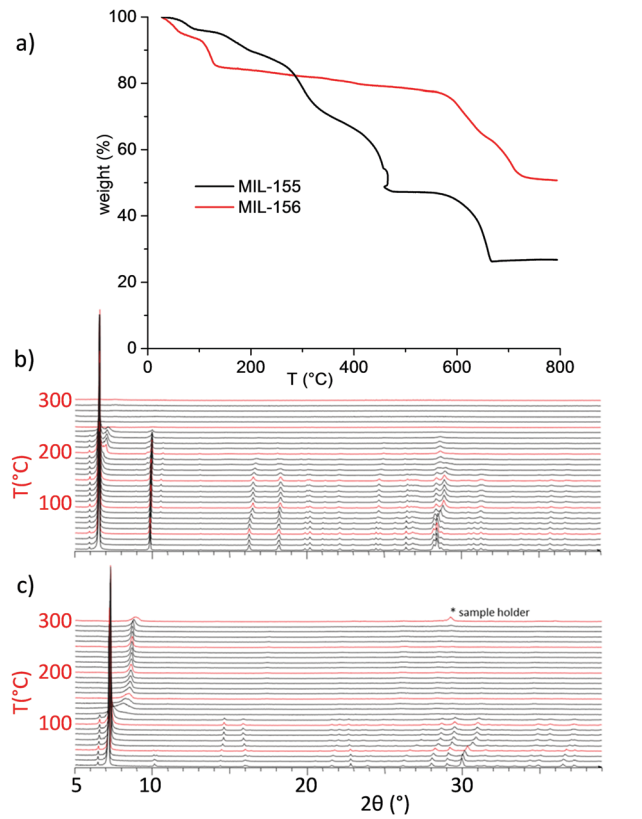

Fig. 3 Thermal behaviour of MIL-155 and MIL-156: (a) thermogravimetric analyses (under O_2); (b and c) temperature dependent powder XRD analysis of MIL-155 and MIL-156 respectively (under air).

by flow cytometry. A third control, namely the basal control C_{basal}, in which the cells were subjected to no treatment at all (neither the ROS inducer nor the ROS reactant) was also considered (see the Experimental section). The results are

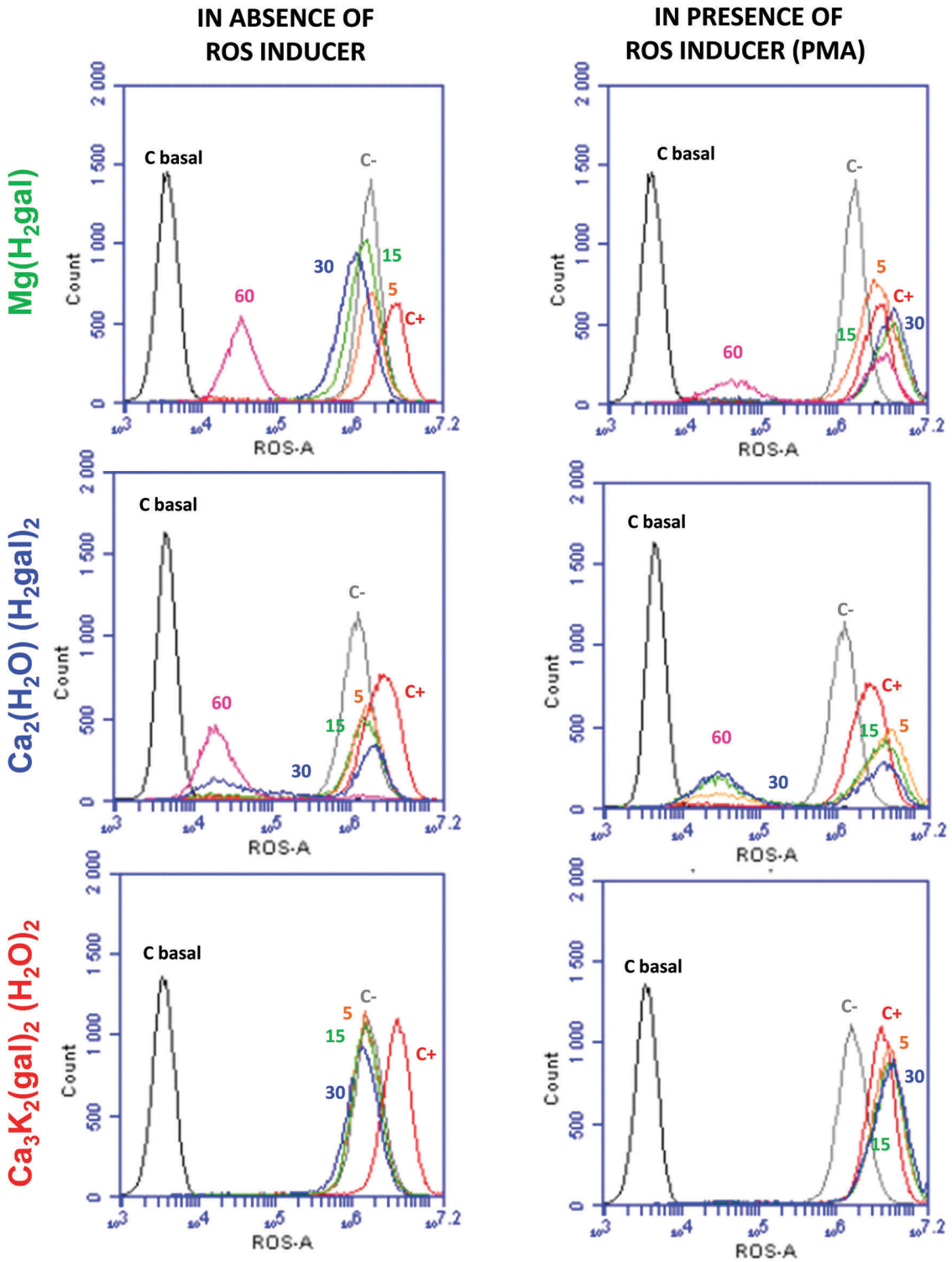

Fig. 4 ROS production of HL-60 cells in contact with $Mg(H_2gal)$ (top), MIL-155 (middle) and MIL-156 (bottom). Basal (cells), negative (cells + DCFH-DA) and positive (cells + DCFH-DA + PMA) controls are disclosed as black, grey and red lines, respectively. Several concentrations (5, 15, 30 and 60 μg mL^{-1}) were tested, and are pictured in orange, green, blue and pink, respectively. Note that these data, corresponding to one of the triplicates obtained in four independent experiments (n = 12), are totally representative from the whole results. Left and right sides correspond to the cells with or without a ROS inducer (PMA), respectively.

summarised in Fig. 4, left. Interestingly, while almost no change of the ROS production compared to the negative control was detected for MIL-156 whatever the concentration, a second peak shifted towards the basal control occurs for MIL-155, being consistent with a concentration-dependent antioxidant activity (Fig. 4, left). With the aim of elucidating the role of both gallate and calcium constituents, the ROS activity was determined for the synthesis precursors (Fig. S7, ESI†). If none of the calcium precursors ($Ca(OH)_2$ and $Ca(NO_3)_2$) lead to a significant effect on the oxidation state of the cells, the gallic acid showed, as expected,[43] a noticeable antioxidant effect. As MIL-155 and MIL-156 are built up from the same constituents, further studies were carried out to understand their drastically different antioxidant activity. The chemical stabilities of both solids were evaluated by suspending the solids in different media at 37 °C: (i) a simple aqueous solution was used to mimic the degradation of the solids under cutaneous administration, considering their potential cosmetic interest; and (ii) cell culture medium (RPMI), in order to correlate the observed antioxidant activity with the release rate of the constitutive components of the solids into the cellular environment, where the antioxidant assays took place. After 24 h of incubation, the chemical degradation was evaluated by means of the gallate ligand release into the media, determined by HPLC (see the Experimental section).

Remarkably, as shown in Fig. 5, while MIL-156 exhibits a high chemical stability regardless of the media, with almost no release of its constitutive gallate ligand to the media (0.05 ± 0.01 *vs.* 0.4 ± 0.1% in water and RPMI, respectively), MIL-155 progressively degrades within water and RPMI (after 24 h, 27 ± 12% and 48 ± 22, respectively). Such a difference in solubility can be related to their different crystal structures: MIL-156 is built up from a fully deprotonated ligand (gal^{4-}), whereas MIL-155 possesses a less negatively charged ligand (H_2gal^{2-}), resulting in stronger ligand-cation bonds for MIL-156. This is confirmed by the comparison of MIL-155 and $Mg(H_2gal)$: despite the different nature and coordination sphere of the cation, the same protonation state for the ligand leads to very similar dissolution profiles, regardless of the media (Fig. 5). Eventually, the absence of dissolution of MIL-156 explains the lack of antioxidant activity of this solid, confirming that the effect is associated with the release of the gallate ligand into the media.

In this line, the present concentration-dependent antioxidant activity supports the fact that the antioxidant effect is due to the progressive delivery of its constituents. More precisely, depending on the dose of MIL-155, we can remarkably observe the emergence of a double cell population related to a different oxidation state, being more prominent from 30 μg mL^{-1} (Fig. 4, right). While the oxidation state of a fraction of the cells is not affected by the presence of MIL-155, the ROS of the other cell population is notably shifted to the negative control values, even reaching a similar oxidation state than the basal control. The proportion of this last population strongly depends on the dose of the solid in contact with the HL-60 cells. These observations suggest that the amount of gallate released from the material degradation is not able to affect the total pull of cells, but only a fraction. Therefore, the antioxidant effect would depend not only on the material concentration but also on its degradation rate (time-dependent effect).

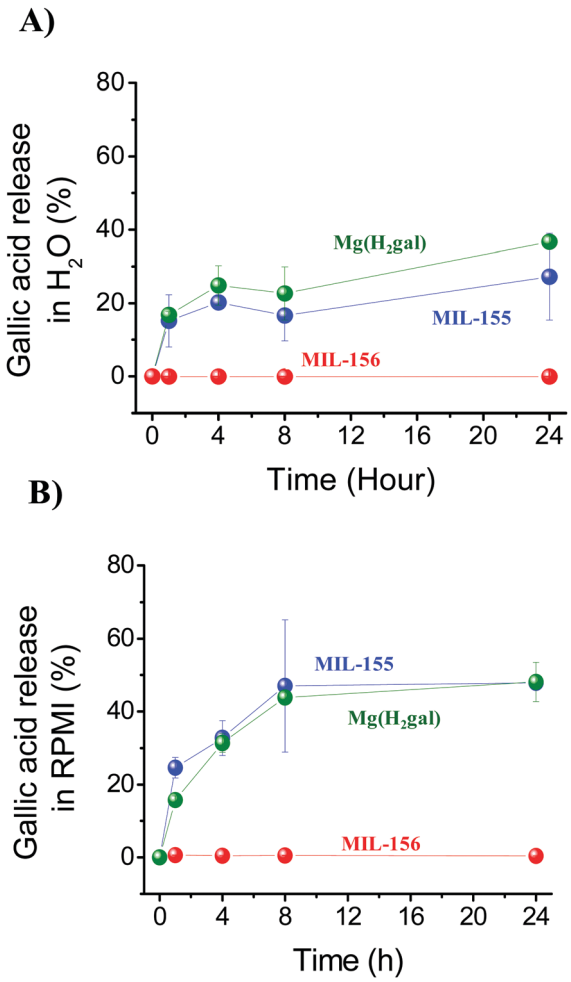

Fig. 5 Degradation profile of $Mg(H_2gal)$, MIL-155 and MIL-156 in aqueous and cell culture media (RPMI) at 37 °C.

In parallel, the potential oxidative protective effect of the calcium gallates was also evaluated in the presence of oxidant species by keeping in contact the cells with different doses of MOF in the presence of PMA, a ROS inducer (Fig. 4, right). As expected, MIL-156 exhibits a similar ROS production than the positive control, in agreement with the absence of antioxidant activity due to its high chemical stability. Interestingly, MIL-155 demonstrates a significant antioxidant protective effect, dependent on the concentration. If one compares these results with the previously reported $Mg(H_2gal)$,[43] also exhibiting a protective antioxidant activity, one can notice a higher efficacy for MIL-155. Indeed, while only the highest tested doses of $Mg(H_2gal)$ (60 μg mL^{-1}) show antioxidant activity, MIL-155 shows a protective activity at much lower concentrations (from 5 μg mL^{-1}; Fig. 4, right). If one considers the concentration of released gallate in solution, very similar amounts are detected within the medium for both solids (0.17 *vs.* 0.19 μg mL^{-1} for MIL-155 and $Mg(H_2gal)$, respectively). This suggests an influence of the cation on the oxidant effect. In contrast to magnesium, calcium is

known to be indirectly involved in the ROS balance. Indeed, high intracellular calcium levels can induce ROS production, which is associated with the disruption of the mitochondrial membrane, and consequently, with cell apoptosis.[57,58] However, this seems to be in contradiction with our findings, evidencing a lower ROS. Although more specific studies are needed to elucidate the antioxidant mechanism, one could hypothesise that the presence of the gallate linker can also modify the intracellular calcium levels (by coordination, for instance).

Conclusions

Two new 3-D coordination polymers, namely MIL-155 and MIL-156, built up from both Ca and gallic acid were prepared, and their crystal structures were determined; both solids exhibit a suitable biocompatibility, as evidenced by the high cell viability and the low presence of apoptotic cells when several cell lines were incubated with the solids. While made of the same constituents, these solids exhibit different composition and crystal structures, leading to very distinct solubility profiles in relevant simulated biological media and hence different biological activities. Whereas MIL-156 does not present any antioxidant effect because of its high chemical stability, the progressive release of the gallate ligand from the less stable MIL-155 leads to a remarkable protective antioxidant effect, which is even higher than those previously reported for the $Mg(H_2gal)$ material. Hence, antioxidant based MOFs appear to be promising candidates not only for bioapplications (*e.g.* dermatology, skin treatment such as wound healing,[59] skin-whitening in cosmetics due to its inhibitory activity against melanogenesis[60]) but also for food preservation (*e.g.* antimicrobial activity,[61] prevention of lipid oxidation[62]), smart surfaces[63,64] or cancer therapy (*e.g.* inhibition of carcinogenesis,[65] prevention of lung cancer[66]), among others, with their crystallochemistry being as important as their composition in determining their activity.

Contribution of the authors

LC, MG, GM, CS, and TD: synthesis and solid state characterisation. JM, NG, and PF: XRD structural studies. TH, TGF, RSV, AGF, and PH: stability, toxicity and bioactivity studies. TD and PH: management of the project, writing of the synthesis/characterisation and bioactivity parts, respectively.

Acknowledgements

This work was supported by a grant (PhD fellowship L. Cooper) from the Région Ile-de France, which is warmly acknowledged, as well as by the UVSQ, CNRS, and by two public grants overseen by the French National Research Agency (ANR), the ANR 2010-MatePro VirMIL and the Laboratoire d'Excellence Nano-Saclay (ref: ANR-10-LABX-0035) as part of the "Investissements d'Avenir" program. Camille Olivier is acknowledged for preliminary experimental studies. PH acknowledges the Spanish Ramon y Cajal Programme (grant agreement no. 2014-16823) and the People Programme (Marie Curie Actions) of the European Union's Seventh Framework Programme (FP7/2007-2013) under REA grant agreement no. 291803. The authors thank the synchrotron Soleil for providing access to the beamline CRISTAL.

Notes and references

1 Special issue, *Chem. Soc. Rev.*, 2009, **38**(5).
2 Special issue, *Chem. Rev.*, 2012, **112**(2).
3 Special issue, *Chem. Soc. Rev.*, 2014, **43**(16).
4 J. Della Rocca, D. Liu and W. Lin, *Acc. Chem. Res.*, 2011, **44**, 957.
5 P. Horcajada, R. Gref, T. Baati, P. K. Allan, G. Maurin, P. Couvreur, G. Férey, R. E. Morris and C. Serre, *Chem. Rev.*, 2012, **112**, 1232.
6 M. Giménez-Marqués, T. Hidalgo, C. Serre and P. Horcajada, *Coord. Chem. Rev.*, 2016, **307**, 342.
7 P. Horcajada, C. Serre, M. Vallet-Regí, M. Sebban, F. Taulelle and G. Férey, *Angew. Chem., Int. Ed.*, 2006, **45**, 5974.
8 K. M. L. Taylor, W. J. Rieter and W. Lin, *J. Am. Chem. Soc.*, 2008, **130**, 14358.
9 L. L. Wen, F. Wang, X. K. Leng, C. G. Wang, L. Y. Wang, J. M. Gong and D. F. Li, *Cryst. Growth Des.*, 2010, **10**, 2835.
10 X. Zhu, H. Zheng, X. Wei, Z. Lin, L. Guo, B. Qiu and G. Chen, *Chem. Commun.*, 2013, **49**, 1276.
11 V. Lykourinou, Y. Chen, X. S. Wang, L. Meng, T. Hoang, L. J. Ming, R. L. Musselman and S. Ma, *J. Am. Chem. Soc.*, 2015, **133**, 10382.
12 S. R. Miller, D. Heurtaux, T. Baati, P. Horcajada, J. M. Grenèche and C. Serre, *Chem. Commun.*, 2010, **46**, 4526.
13 L. N. Duan, Q. Q. Dang, C. Y. Han and X. M. Zhang, *Dalton Trans.*, 2015, **44**, 1800.
14 R. C. Huxford, K. E. de Krafft, W. S. Boyle, D. Liu and W. B. Lin, *Chem. Sci.*, 2012, **3**, 198.
15 C. Serre, F. Millange, S. Surblé and G. Férey, *Angew. Chem., Int. Ed.*, 2004, **43**, 6285.
16 L. Xing, H. Zheng and S. Che, *Chem. – Eur. J.*, 2011, **17**, 7271.
17 I. Imaz, M. Rubio-Martinez, J. An, I. Sole-Font, N. L. Rosi and D. Maspoch, *Chem. Commun.*, 2011, **47**, 7287.
18 R. P. Heaney, K. M. Davies and M. J. Barger-Lux, *J. Am. Coll. Nutr.*, 2002, **21**, 152.
19 R. P. Heaney, *Am. J. Clin. Nutr.*, 2008, **88**, 541.
20 S. Forsen and J. Kordel, *Bioinorg. Chem.*, 1994, 107.
21 M. W. Berchtold, H. Brinkmeier and M. Muntener, *Physiol. Rev.*, 2000, **80**, 1215.
22 M. B. Zemel, *J. Am. Coll. Nutr.*, 2001, **20**, 440.
23 J. An, R. P. Fiorella, S. J. Geib and N. L. Rosi, *J. Am. Chem. Soc.*, 2009, **131**, 8401.
24 N. Guillou, C. Livage, M. Drillon and G. Férey, *Angew. Chem., Int. Ed.*, 2003, **42**, 5314.
25 M. Gaab, N. Trukhan, S. Maurer, R. Gummaraju and U. Müller, *Microporous Mesoporous Mater.*, 2012, **157**, 131.
26 G. Wissmann, A. Schaate, S. Lilienthal, I. Bremer, A. M. Schneider and P. Behrens, *Microporous Mesoporous Mater.*, 2012, **152**, 64.

27 R. A. Smaldone, R. S. Forgan, H. Furukawa, J. J. Gassensmith, A. M. Z. Slawin, O. M. Yaghi and J. F. Stoddart, *Angew. Chem., Int. Ed.*, 2010, **49**, 8630.
28 J. Rabone, Y. F. Yue, S. Y. Chong, K. C. Stylianou, J. Bacsa, D. Bradshaw, G. R. Darling, N. G. Berry, Y. Z. Khimyak, A. Y. Ganin, P. Wiper, J. B. Claridge and M. J. Rosseinsky, *Science*, 2010, **329**, 1053.
29 T. Jahnert, M. D. Hager and U. S. Schubert, *J. Mater. Chem. A*, 2014, **2**, 15234.
30 B. S. Mendiguchia, I. Aiello and A. Crispini, *Dalton Trans.*, 2015, **44**, 9321.
31 T. Marino, A. Galano and N. Russo, *J. Phys. Chem. B*, 2014, **118**, 10380.
32 N. Niho, M. Shibutani, T. Tamura, K. Toyoda, C. Uneyama, N. Takahashi and M. Hirose, *Food Chem. Toxicol.*, 2001, **39**, 1063.
33 J. M. Kratz, C. R. Andrighetti-Fröhner, P. C. Leal, R. J. Nunes, R. A. Yunes, E. Trybala, T. Bergstrom, C. R. M. Barardi and C. M. O. Simoes, *Biol. Pharm. Bull.*, 2008, **31**, 903.
34 M. S. Kang, J. S. Oh, I. C. Kang, S. J. Hong and C. H. Choi, *J. Microbiol.*, 2008, **46**, 744.
35 H. M. Chen, Y. C. Wu, Y. C. Chia, F. R. Chang, H. K. Hsu, Y. C. Hsieh, C. C. Chen and S. S. Yuan, *Cancer Lett.*, 2009, **286**, 161.
36 M. Kaur, B. Velmurugan, S. Rajamanickam, R. Agarwal and C. Agarwal, *Pharm. Res.*, 2009, **26**, 2133–2140.
37 D. H. Priscilla and P. S. Prince, *Chem.-Biol. Interact.*, 2009, **179**, 118.
38 Z. B. Lu, G. J. Nie, P. S. Belton, H. R. Tang and B. L. Zhao, *Neurochem. Int.*, 2006, **48**, 263.
39 L. Cooper, N. Guillou, C. Martineau, E. Elkaim, F. Taulelle, C. Serre and T. Devic, *Eur. J. Inorg. Chem.*, 2014, 6281–6289.
40 G. Mouchaham, L. Cooper, N. Guillou, C. Martineau, E. Elkaim, S. Bourrelly, P. L. Llewellyn, C. Allain, G. Clavier, C. Serre and T. Devic, *Angew. Chem., Int. Ed.*, 2015, **54**, 13297.
41 R. K. Feller and A. K. Cheetham, *Solid State Sci.*, 2006, **8**, 1121.
42 P. J. Saines, H. H. M. Yeung, J. R. Hester, A. R. Lennie and A. K. Cheetham, *Dalton Trans.*, 2011, **40**, 6401.
43 L. Cooper, T. Hidalgo, M. Gorman, T. Lozano-Fernandez, R. Simon-Vazquez, C. Olivier, N. Guillou, C. Serre, C. Martineau, F. Taulelle, D. Damasceno-Borges, G. Maurin, A. Gonzalez-Fernandez, P. Horcajada and T. Devic, *Chem. Commun.*, 2015, **51**, 5848.
44 Sigma-Aldrich Home Page. http://www.sigmaaldrich.com/lifescience/cellculture/learning-center/media-formulations/rpmi-1640.html (accessed 2013).
45 G. Mradu, S. Saumyakanti, M. Sohini and M. Arup, *Int. J. Pharm. Phytopharm. Res.*, 2012, **4**, 162.
46 S. G. Verza, C. Pavei and G. G. Ortega, *J. Braz. Chem. Soc.*, 2008, **19**, 1627.
47 E. Bellido, T. Hidalgo, M. V. Lozano, M. Guillevic, R. Simon-Vazquez, M. J. Santander-Ortega, A. Gonzalez-Fernandez, C. Serre and M. J. Alonso andP. Horcajada, *Adv. Healthcare Mater.*, 2015, **4**, 1246.
48 B. Kong, J. H. Seog, L. M. Graham and S. B. Lee, *Nanomedicine*, 2011, **6**, 929.
49 C. Tamames-Tabar, D. Cunha, E. Imbuluzqueta, F. Ragon, C. Serre, M. J. Blanco-Prieto and P. Horcajada, *J. Mater. Chem. B*, 2014, **2**, 262.
50 Y. Shounan, X. Feng and P. J. O'Connell, *J. Immunol. Methods*, 1998, **217**, 61.
51 M. van Engeland, L. J. W. Nieland, F. C. S. Ramaekers, B. Schutte and C. P. M. Reutelingsperger, *Cytometry*, 1998, **31**, 1.
52 S. H. Mehta, R. C. Webb, A. Ergul, A. Tawak and A. M. Dorrance, *Am. J. Physiol.: Regul., Integr. Comp. Physiol.*, 2004, **286**, 505.
53 A. Aranda, L. Sequedo, L. Tolosa, G. Quintas, E. Burello, J. V. Castellad and L. Gombau, *Toxicol. In Vitro*, 2013, **27**, 954.
54 P. M. Forster, A. R. Burkbank, C. Livage, G. Férey and A. K. Cheetham, *Chem. Commun.*, 2004, 368.
55 D. A. Dougherty, *Acc. Chem. Res.*, 2013, **4**, 885.
56 S. Quideau, D. Deffieux, C. Douat-Casassus and L. Pouységu, *Angew. Chem., Int. Ed.*, 2011, **50**, 586.
57 C. C. Huang, R. S. Aronstam, D. R. Chen and Y. W. Huang, *Toxicol. In Vitro*, 2010, **24**, 45.
58 V. Voccoli, I. Tonazzini, G. Signore, M. Caleo and M. Cecchini, *Cell Death Dis.*, 2014, **5**, 1529.
59 D. J. Yang, S. H. Moh, D. H. Son, S. You, A. W. Kinyua, C. M. Ko, M. Song, J. Yeo, Y. H. Choi and K. W. Kim, *Molecules*, 2016, **21**, 899, DOI: 10.3390/molecules21070899.
60 H. J. Roh, H. J. Noh, C. S. Na, C. S. Kim, K. H. Kim, C. Y. Hong and K. R. Lee, *Biomol. Ther.*, 2015, **23**, 283.
61 T. Hintz, K. K. Matthews and R. Di, *BioMed Res. Int.*, 2015, 246264.
62 S. Maqsood, S. Benjakul, A. Abushelaibi and A. Alam, *Compr. Rev. Food Sci. Food Saf.*, 2014, **13**, 1125.
63 I. A. Jankovic, Z. V. Saponjic, E. S. Dzunuzovic and J. M. Nedeljkovic, *Nanoscale Res. Lett.*, 2010, **5**, 81.
64 Z. Yang, K. Xiong, P. Qi, Y. Yang, Q. Tu, J. Wang and N. Huang, *ACS Appl. Mater. Interfaces*, 2014, **6**, 2647.
65 S. Vermaa, A. Singhb and A. Mishra, *Environ. Toxicol. Pharmacol.*, 2013, **35**, 473.
66 B. C. Ji, W. H. Hsu, J. S. Yang, T. C. Hsia, C. C. Lu, J. H. Chiang, J. L. Yang, C. H. Lin, J. J. Lin, L. J. W. Suen, W. G. Wood and J. G. Chung, *J. Agric. Food Chem.*, 2009, **57**, 7596.

